Intelligent and Converged Networks
2020, 1(1): 37–57

ISSN 2708-6240
DOI: 10.23919/ICN.2020.0002

Internet of radio and light: 5G building network radio and edge architecture

Yue Zhang*, Hequn Zhang, John Cosmas, Nawar Jawad, Kareem Ali, Ben Meunier, Adam Kapovits, Li-Ke Huang, Wei Li, Lina Shi, Xun Zhang, Jintao Wang, Israel Koffman, Muller Robert, and Charilaos C. Zarakovitis

Abstract: The Internet of Radio-Light (IoRL) is a cutting-edge system paradigm to enable seamless 5G service provision in indoor environments, such as homes, hospitals, and museums. The system draws on innovative architectural structure that sits on the synergy between the Radio Access Network (RAN) technologies of millimeter Wave communications (mmWave) and Visible Light Communications (VLC) for improving network throughput, latency, and coverage compared to existing efforts. The aim of this paper is to introduce the IoRL system architecture and present the key technologies and techniques utilised at each layer of the system. Special emphasis is given in detailing the IoRL physical layer (Layer 1) and Medium Access Control layer (MAC, Layer 2) by means of describing their unique design characteristics and interfaces as well as the robust IoRL methods of improving the estimation accuracy of user positioning relying on uplink mmWave and downlink VLC measurements.

Key words: 5G; Internet of Radio-Light (IoRL); Visible Light Communications (VLC); millimeter Wave communications (mmWave); Remote Radio Light Head (RRLH); Network Function Virtualization (NFV); Software Defined Network (SDN); positioning

1 Introduction

The development of the Fifth Generation (5G) mobile and wireless networks has progressed at a rapid pace. The European Union (EU) funds 5G Public Private Partnership (5GPPP) Phases 1 and 2 projects that have played an important role in establishing a pre-standardisation consensus on areas ranging from physical layer to overall architecture, network management, and software networks. The 5G system has the ambition of responding to the widest range of services and applications in the history of mobile and wireless communications categorised in enhanced Mobile Broad Band (eMBB), Ultra-Reliable and Low-Latency Communications (URLLC), and massive Machine-Type Communications (mMTC) by various technologies including massive Multiple-Input-Multiple-Output (mMIMO), millimeter Wave communications (mmWave), Visible Light Communciation (VLC), and massive Internet of Things (IoT)[1–3]. The Internet of Radio-Light (IoRL) system architecture[4–7] is a layered construction consisting of four layers, namely, service layer, Network Function Virtualization (NFV) layer, Software Defined Network (SDN) layer, and access layer, as illustrated in Fig. 1. Such an architecture is

• Yue Zhang and Hequn Zhang are with the School of Engineering, University of Leicester, Leicester, LE1 7RH, UK. E-mail: Yue.Zhang@Leicester.ac.uk; hz148@leicester.ac.uk.
• John Cosmas, Nawar Jawad, Kareem Ali, and Ben Meunier are with Brunel University, London, UB8 3PH, UK. E-mail: John.Cosmas@Brunel.ac.uk; Nawar.Jawad@brunel.ac.uk; Kareem.Ali@brunel.ac.uk; Benjamin.Meunier@brunel.ac.uk.
• Adam Kapovits is with Eurescom GmBH, Heidelberg 69123, Germany. E-mail: kapovits@eurescom.eu.
• Li-Ke Huang and Wei Li are with Viavi Solutions, Stevenage, SG1 2AN, UK. E-mail: Li-Ke.huang@Viavisolutions.com; Wei.Li@Via.visolutions.com.
• Lina Shi and Xun Zhang are with Institut Supérieur D'électronique De Paris, Paris 75006, France. E-mail: lina.shi@ isep.fr; xun.zhang@isep.fr.
• Jintao Wang is with Department of Electronic Engineering, Tsinghua University, Beijing 100084, China. E-mail: wangjitao@tsinghua.edu.cn.
• Israel Koffman is with RunEL Ltd, Rishon Lezion 7565502, Israel. E-mail: israelk@runel.net.
• Muller Robert is with Fraunhofer IIS, Ilmenau 98693, Germany. E-mail: mueller.robert@tu-ilmenau.de.
• Charilaos C. Zarakovitis is with National Centre of Scientific Research Demokritos, Agia Paraskevi 15341, Greece. E-mail: c.zarakovitis@iit.demokritos.gr.
* To whom correspondence should be addressed.
Manuscript received: 2020-02-17; accepted: 2020-03-05

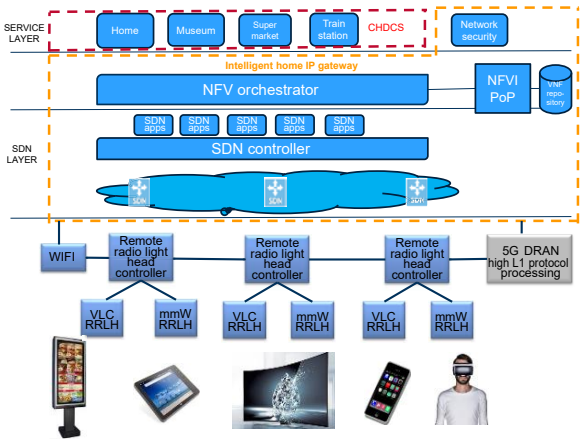

Fig. 1 IoRL layered architecture.

more akin to a radio-light home eNodeB suitable for a single building network rather than an Evolved Packet Core (EPC) suitable for a whole country. All four layers can be deployed inside the 5G Mobile Edge Computing (MEC) server, which can be used for the Artificial Intelligence (AI) and Machine Learning (ML) driven control of the eMBB and URLLC user cases for indoor environments[8].

The service layer is to (1) run server side applications for streaming audio and video, (2) receive and store results on databases and monitor security from a multi-core Cloud Home Data Centre Server (CHDCS), and (3) run mobile applications from User Equipment (UE), i.e., smart phones, tablet Personal Computers (PCs), Virtual Reality (VR) and Augmented Reality (AR) headsets, and High Definition Televisions (HDTVs).

The processing of 5G Medium Access Control (MAC) layer and Remote Radio Control (RRC) layer is running on a remote server. In this paper, the MAC layer and RRC layer are also named as Layers 2 and 3 for short, respectively, and the server where they locate at is called Layers 2&3 server. This remote server needs to connect with the SDN layer through the internet. Because of this, an SDN Forwarding Device (FD) is needed to reside within the SDN layer to route Internet Protocol (IP) packets between the Layers 2&3 server and the SDN server. Thereby, the Network Function Virtualization Orchestrator (NFVO) invokes various Virtual Network Functions (VNFs) required for shaping an Intelligent Home IP Gateway (IHIPG) that enables local access and mobility management, deep packet inspection, and transcoding processes for video streaming and network security functions, etc. Layers 2 and 3 are responsible for radio resource allocation and intra building handover. It receives/sends user IP packets from/to SDN by Transmission Control Protocol (TCP)/IP packets. For downlink, each TCP/IP packet contains a Quality-of-Service (QoS) Flow Identification (QFI) defined within IP header. With a pre-defined QoS table defined in the RRC layer, it can decide a radio resource allocation scheme for the destination UE. Between the Layer 2 and the access layer, the User Datagram Protocol (UDP) and IP packets are adopted to deliver the control and user data. With positioning information and Signal Quality Indicators (SQI) gathered from the lower layer, intra building handover processing can be implemented to handover a UE from one Remote Radio Light Head (RRLH) to another RRLH within a building.

Moreover, the access layer can consist of up to thirty two RRLH controllers providing a total of 10 Gbit/s to a single building between them. As shown in Fig. 2, each RRLH controller drives up to four VLC and mmWave RRLH pairs with the same transmission block sub-frame, thereby providing a Multiple Input Single Output (MISO) transmission on downlink paths and a Single Input Multiple Output (SIMO) on uplink paths for its coverage area, which is typically a room or floor area of a building.

In the IoRL system, a UE can obtain direct access to the internet or the 5G core and gNodeB through a cloud gateway. Thereby, the system facilitates handover between the outside 5G network and the indoor 5G

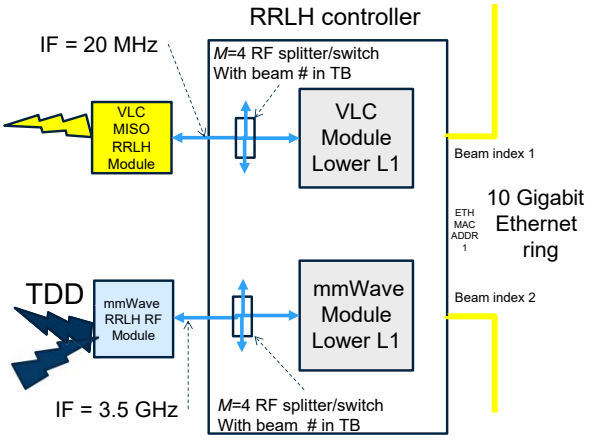

Fig. 2 RRLH architecture with external WLAN.

network[9]. Hence, the proposed system architecture can enable building owners to connect to multiple different operators, use multiple different devices registered to different operators, and exploit license-free spectrum for accessing the internet or mobile network using the home network.

Other parts of the paper are organized as follows. In Section 2, a 5G building network Radio Access Network (RAN) architecture is introduced. Then, the RRC and intra building handover are introduced in Section 3. Location estimation architecture is presented in Section 4. The RAN testbed for mmWave and VLC and the measurement method are introduced in Section 5. Measurement results are presented and discussed in Section 6. Positioning sensing simulation is presented in Section 7. This paper concludes in Section 8.

2 5G building network RAN architecture

As illustrated in Fig. 1, the IoRL access layer uses an enhanced Common Public Radio Interface (eCPRI) Ethernet ring to interconnect an upper Layer 1 processing on a Field-Programmable Gate Array (FPGA) with up to thirty two RRLH controller FPGAs each hosting two lower Layer 1 processors. The first controller generates an Intermediate Frequency (IF) signal to drive up to 4 VLC MISO modules using a 1 to 4 Radio Frequency (RF) splitter/switch. The 1 to 4 means that with that splitter, an input signal can be split into 4 output signals. The second controller generates an IF signal to drive or be driven by up to 4 mmWave RF Duplex modules using a 1 to 4 RF splitter/switch.

The functional split between the RRLH remote unit and the central unit in the physical Layer 1 is at split 7 on the protocol stack[10]. The eCPRI Ethernet ring is looped from room to room in a building from one RRLH controller to another in a similar way to the electric light circuit in a home.

A 10 MHz reference clock signal is generated locally and sent to each mmWave RRLH module for use in 5G synchronisation, thereby leaving just amplification and IF to RF up conversion to be performed at the RRLH.

As there is a limited space available for 5G communication signal processing in light rose housing within which the VLC and mmWave RRLH are housed, the concepts of NFV and parallel processing pipeline are adopted to offload the processing power and complexity of the communication protocol processing required in the RRLH onto the IHIPG or CHDCS.

Direct Current Orthogonal Frequency Division Multiplexing Access (DC-OFDM) modulation is used for VLC transmission, which is compatible with the New Radio (NR) 5G frame formats[11, 12]. The bandwidth of common VLC Light Emitting Diodes (LEDs) is up to 10 MHz, but this can potentially be extended to 100 MHz depending on the quality of the LEDs' lights used (could be even much higher when LED-based illumination technology becomes mature and utilized), which means that Sub-Carrier Spacing (SCS) of 15, 30, and 60 kHz from the 5G NR Frequency Range (FR) 1 frame formats (FR1) can be used[13], potentially providing maximum downlink bitrate of 691.2 Mbit/s when 256-Quadrature Amplitude Modulation (QAM) and 100 MHz bandwidth are used. Since the IoRL project intends to use VLC LEDs of 10 MHz bandwidth and SCS of 60 kHz, then it will provide a maximum downlink bitrate of 56.32 Mbit/s (not taking into account the signaling overhead). The NR FR2 frame format defined in Ref. [13] can use much higher bandwidths of up to 400 MHz by using SCS of 60 or 120 kHz and be operated in 60 GHz unlicensed spectrum, thereby providing uplink and downlink bit rates ranging up to 2.7 Gbit/s, when using 256-QAM and 100 MHz bandwidth, depending on the Time Division Duplex (TDD) frame type used. Since the IoRL system uses mmWave bandwidth of 100 MHz and SCS of 60 kHz, it is likely to provide a maximum downlink or uplink bitrate of 675.84 Mbit/s (not taking into account the signaling overhead).

MISO diversity is used in the downlink, where the same data are transmitted from different mmWave antennas and VLC LEDs by the RRLHs at the same time using an RF splitter, which increases transmission reliability. In effect, this creates a man-made multipath environment, where if one or more of VLC or mmWave paths are occluded, then the other paths can be always available, ensuring the continuation of communications. SIMO diversity is used in the uplink, where the same data are received by different mmWave antennas at the

RRLHs and maximum ratio combined higher up in the layered protocol, which further enhances transmission reliability.

In case where all paths are occluded, e.g., when a user conceals the Photo Diode (PD) receiver and mmWave antenna at the UE, then Multi Source (MS) streaming[14] is enabled to ensure that there is always the availability of another low capacity Wireless Local Area Network (WLAN) path for the continuation of communications and synchronisation with the streaming audio/video. Also, the IoRL IHIPG uses a deep packet inspection NFV function to identify video streams and video transcoding for generating a lower-quality Multi Source Stream (MSS) for the WLAN path to the UE, whereas the original higher-quality HDTV stream is transmitted by the broadband radio-light network[14]. This concept can be applied on either multipath TCP or UDP protocols for video streaming.

For example, the parallelization of cutoff pair interactions is mature on CPUs, and typically employs a voxel-based method.

3 Radio resource control and intra building handover

3.1 Overview

Based on the functions of Layers 2 and 3, the main components of the IoRL radio resource control are listed below:

(1) Layers 1 and 2 interface handles the UDP/IP packets between these layers.

(2) Layer 2, Layer 3, and SDN interface handles the TCP/IP packets transmitted between Layers 2 and 3 server and the SDN server in both the downlink and uplink. For the downlink, the interface needs to read QoS Flow Identification (QFI) information from the IP header of TCP/IP and the Identification (ID) data of the destination UE for the radio resource control in RRC layer, and pass the user data down to the lower layers. For uplink, the interface puts the user data into TCP/IP packets and sends them to SDN server.

(3) RRC layer controls the radio resources and intra handover. A radio resource allocation scheme can be decided by the QFI and a pre-defined QoS table. The intra handover procedure should be defined here and the strategy of it should be based on the positioning and SQI information.

(4) Packet Data Convergence Protocol (PDCP) / Radio Link Control (RLC) / MAC sub-layers are mainly responsible for packing Protocol Data Units (PDUs) in each sub-layer and mapping the corresponding PDUs to the channels. These sub-layers will be implemented based on the 3GPP 38 series.

The following subsections introduce the IoRL achievements at the current stage.

3.2 Layers 1 and 2 interface

For Layers 1 and 2 downlink interface definition, the types and size of data used between Layers 1 and 2 as well as the data transmission procedure are defined. Three types of UDP packets are defined in Layers 1 and 2 interface for user and control data transmission, i.e., the payload packet, the Downlink Control Information (DCI) packet, and the End Of Slot (EOS) packet. The payload packet is used to carry the user data and descriptor information for Physical Downlink Shared Channel (PDSCH). The DCI packet carries descriptor information for Physical Downlink Control Channel (PDCCH). The EOS packet is to inform Layer 1 whether the transmission in current time slot is completed. At the beginning of each slot, the payload packets and the DCI packet of the first UE are delivered, then, of the second UE, and so on. After the packets of all UEs have been sent, the EOS packet is delivered to Layer 1 to inform it that all transmissions in this slot are completed, so that Layer 1 can start processing the radio transmissions.

The workflow of Layers 1 and 2 interface downlink process at Layer 2 side is shown in Fig. 3. It describes the UDP packets' assembly and scheduling process in Layers 1 and 2 interface. The most important point of this procedure is to ensure that the transmission order is correct and all UEs' packets have been sent in short time (much less than one slot).

3.3 Layer 2, layer 3, and SDN interface

The Layer 2, Layer 3, and SDN interface is defined as below:

(1) To simplify the system, the TCP/IP packet is applied to deliver user data between Layer 3 (RRC) and

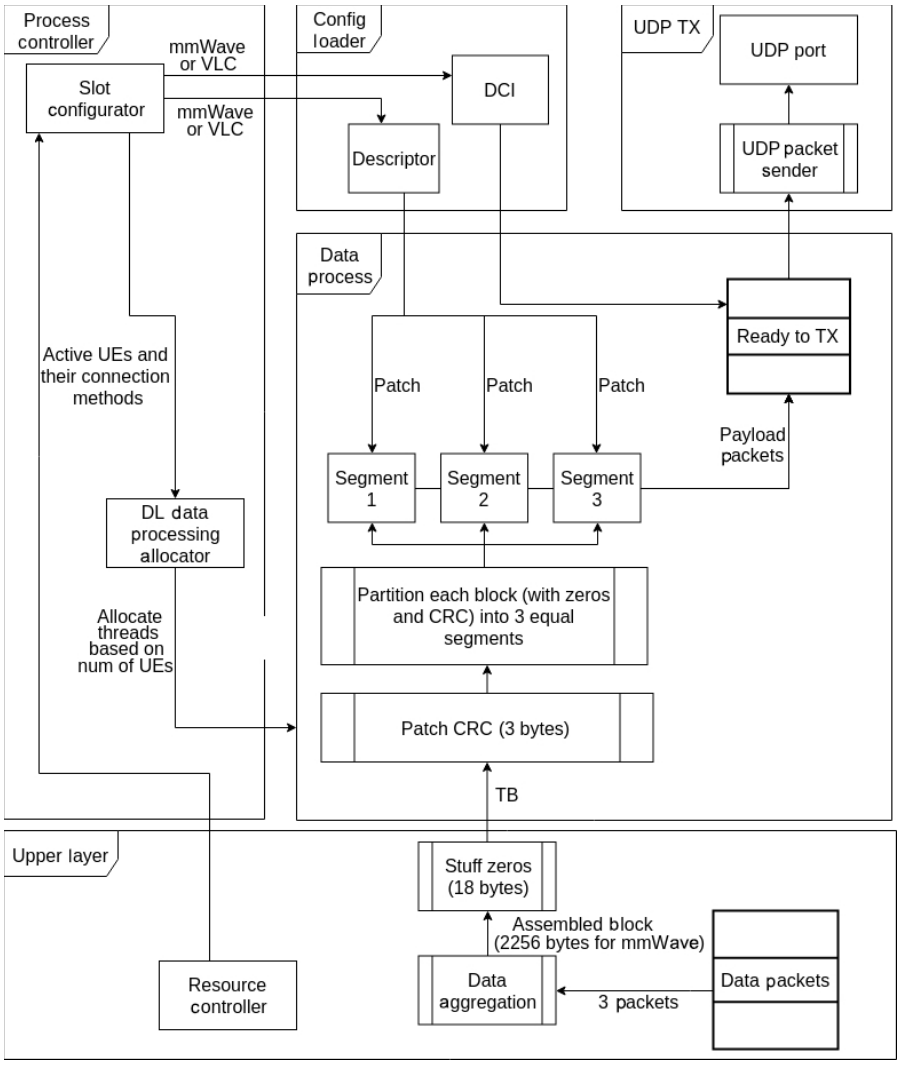

Fig. 3 Workflow of Layers 1 and 2 interface downlink process.

SDN directly, instead of the PDU session.

(2) The destination IP address is used to distinguish different connections between SDN and UEs.

(3) SDN sets QFI into the header of IP packet, which can be read in interface.

(4) A QoS requirement table needs to be pre-defined in RRC layer for radio resources control.

4 Location estimation architecture

4.1 Main components

The main goal of the location estimation architecture is to support the following applications: (1) indoor location-based data access; (2) indoor location monitoring and guiding; (3) interactive location gaming application; and (4) follow-me smart TV service.

The main components of the location estimation architecture are the Location Server (LS), Location Service Client (LSC), RRLH Controller (RRLHC), and Location Database (LD).

LS is in charge of location estimation and represented by a VNF implemented at the IHIPG. LS is actually a Software (SW), which computes position estimates of all UEs that are connected to RRLHs. The computation is based on estimated location relevant signal parameters, coordinates of mmWave antennas, and LEDs situated within RRLHs and floor plans of the environment to enhance the precision.

LSC is represented by application SW, which is situated either at UE or at CHDCS. It requires location information for location-based data access, monitoring and guiding, interactive location gaming application, and follow-me smart TV services.

RRLHC is in charge of location relevant parameter measurement. It directly measures pseudo Time Of Arrival (pTOA) of mmWave Sounding Reference Signals (SRSs). The mmWave pseudo TOA is reported by RRLHC to RRC. RRC communicates the measured parameters to LD using SDN. The VLC Received Signal Strength (RSS) is estimated by UE and communicated to LD using its application SW.

LD is a VNF implemented at IHIPG. It is a MySQL database, which stores three different sets of parameters: (1) location relevant mmWave and VLC parameters of all connected UEs that are measured by RRLHC; (2) estimated location coordinates of all connected UEs; and (3) coordinates of all mmWave antennas and LEDs and also floor plans.

The measured location relevant parameters are written to the database by RRLHCs. The measured location relevant parameters of this data are presented in Table 1. Each entry consists of the UE ID, RRLHC ID, estimated mmWave and VLC parameters, and a timestamp at which the parameters were estimated.

The reason of storing TOA instead of Time Delay Of Arrival (TDOA) measurements, as used conventionally, is to enable unique relation to antenna coordinates. In the TDOA case, a more complex entry would be needed to indicate which two antennas were used to provide TDOA estimate. In the proposed pTOA case, the relation between the antennas coordinates and the pToA_An is given by the Antenna number (An) and the RRLHC ID. The same is valid for the VLC parameters and the relation between LED coordinates and RSS_Ln measurement. The second table in LD contains estimated coordinates by LS. The structure of this data is illustrated in Table 2. Each entry consists of the UE ID, three-dimensional UE coordinates, and a timestamp at which the UE position was estimated. The third table in LD contains antenna and LED coordinates. These coordinates must be saved in LD by the system administrator at the system installation time. The structure of this data is illustrated in Table 3. Each entry consists of RRLHC ID, ID of the RRLH connected to this controller, and antenna and LED coordinates.

The main components of the position sensing architecture are illustrated in Fig. 4. LSC is represented application SW at CHDCS and UEs. There are 3 RRLHCs (RRLH C1, C2, and C3). LS and LD are at IHIPG.

Table 1 Measured location relevant parameters in the location database.

Parameter		Number of bits	Interval
UE ID		8	[0, 255]
RRLH ID		8	[0, 255]
mmWave	pToA_A1	8	[0, 255]
	...	8	[0, 255]
	pToA_An	8	[0, 255]
VLC	RSS_L1	8	[0, 255]
	...	8	[0, 255]
	RSS_Ln	8	[0, 255]
Timestamp		13	MM/dd/yyyy hh:mm:ss a zzz

Table 2 Estimated UE coordinates in the location database.

Parameter		Number of bits	Interval
UE ID		8	[0, 255]
UE coordinate	X	8	[0, 255]
	Y	8	[0, 255]
	Z	8	[0, 255]
Timestamp		13	MM/dd/yyyy hh:mm:ss a zzz

Table 3 Antenna and LED coordinates in the location database.

Parameter		Number of bits	Interval
RRLHC ID		8	[0, 255]
RRLH ID		8	[0, 255]
Antenna coordinate	X	8	[0, 255]
	Y	8	[0, 255]
	Z	8	[0, 255]
LED coordinate	X	8	[0, 255]
	Y	8	[0, 255]
	Z	8	[0, 255]

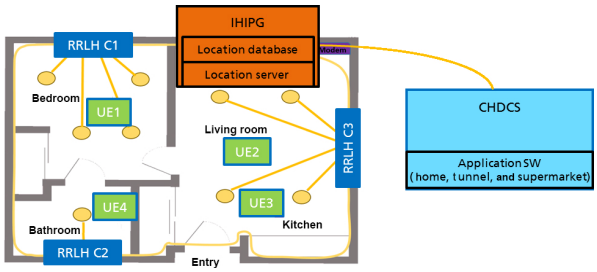

Fig. 4 Main components of the position sensing architecture.

4.2 Communication among the main components of the position sensing architecture

Information exchanges among UEs, RRLHCs, LS, and LSC are performed by exploiting LD. When RRLHC collects a new set of mmWave TOA parameters, it reports them to RRC. RRC communicates these measurements to SDN in the form of packets using PDCP protocol. SDN transfers mmWave location parameters to LD.

When UE collects a new set of VLC RSS parameters, it transfers them to the LD using its Android application SW. LS obtains the measured parameters from LD as well as the location anchoring data represented by coordinates of each mmWave antenna and LED mounted at RRLHs. Coordinates of all connected UEs are estimated by LS and saved in LD. LSCs on the UEs and CHDCS can access the estimated coordinates using LD.

The parameter estimation as well as the computation of UE coordinates are performed continuously by all RRLHCs within the system. When a UE moves into a room either from another room or from outside the building, then the corresponding RRLHC will initiate the location estimation mechanism. On one hand, all RRLHCs and UEs periodically provide results of their location parameter measurements onto the LD. On the other hand, LSCs on the UE and application servers in the CHDCS can assess the location estimates on demand for their applications.

Localisation procedure, which involves interaction between RRLHC and the UE, is enabled by the IoRL Positioning Protocol (IPP). It is an adaptation of the Long Term Evolution (LTE) Positioning Protocol (LPP). The main functions of the IPP are to initiate localisation procedure.

In the mmWave case, RRLH provides UE assistance data (the base sequences, their group, sequence number, cyclic shift, and frequency hopping scheme, etc.) and triggers UE to issue a series of the SRS for uplink TDOA measurements.

In the VLC case, UE triggers the RRLHC to issue a series of reference VLC DC-OFDM symbols for each RRLH in turn for downlink RSS measurements at the UE.

Overview of interactions among the key elements of the positioning architecture is illustrated in Fig. 5. The notation with arrows indicates that the IPP communication is bidirectional. The direction RRLHCs to UE is needed to initiate localization on procedures at the UE, which include transmission of mmWave SRS sequence (see Fig. 6) and measurements of VLC RSS. The opposite direction is needed to initiate VLC RSS measurements at RRLHC from UE.

The Structured Query Language (SQL) IP-based communication with location database is unidirectional for UEs, RRLHCs, and LSC. These components either only provide or only obtain data from the database. The communication between LD and LS is bidirectional. The LS needs measured parameters and location anchor data in order to estimate UE coordinates.

4.3 mmWave RRLH and UE position algorithms

The mmWave parameter measurements are performed by RRLHC in the uplink, whereas the VLC RSS

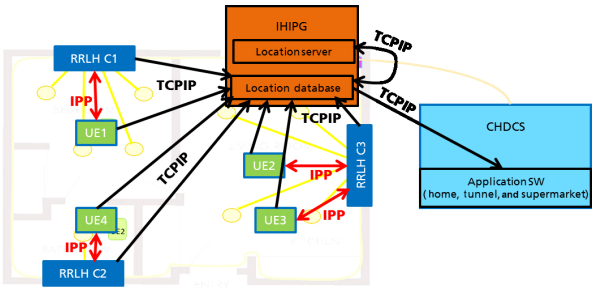

Fig. 5 Communication among the main components of the position sensing architecture.

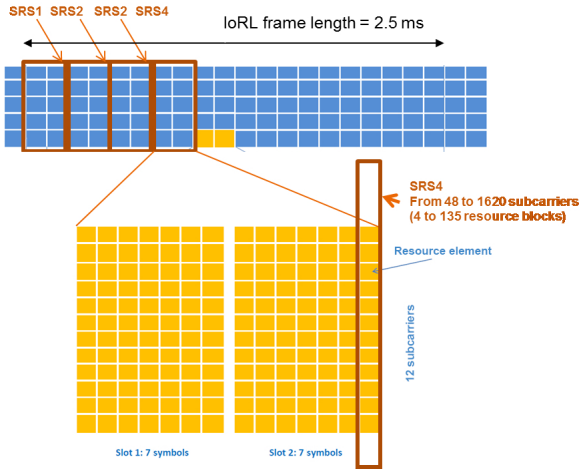

Fig. 6 Generation of mmWave SRS in the generic signal subframe.

measurements are performed by the UE in the downlink.

In the case of mmWave localisation, UE is the transmitter. Firstly, synchronisation between UE (to be localised) and its corresponding RRLHC is established over one of its mmWave antennas. When the synchronisation is established, RRLHC requests UE to transmit a sequence of multiple SRSs. The number of SRSs within the sequence depends on the number of RRLHs connected to the controller. At least four RRLHs are needed for Three-Dimensional (3D) localisation. The timing of partial SRSs within the sequence is a priori known. The SRSs are transmitted within the last symbols of the first four sub-frames of the IoRL signal frame as shown in Fig. 6. With 100 MHz system bandwidth, for each SRS, it will occupy at least 4 resource blocks (48 subcarriers), and the maximum occupied resource blocks can be up to 135 (1620 subcarriers).

Each sub-frame SRS transmission is dedicated to pseudo TOA measurements by one of four RRLHs. The RRLH sequentially measures the pseudo TOAs at each of its RRLHs. The RRLHs are activated sequentially to allow this procedure. This activation is coherent to the SRS timing within the signal frame. At the time, when UE transmits the SRS sequences, the clock of the RRLHC as well as the UE clock will be kept locked. This ensures a coherent time basis for computation of TDOAs according to pseudo TOAs measured with respect to partial SRSs. This procedure is repeated for each UE connected to the RRLHC. The measured location relevant signal parameter is averaged 8 times. Thus, under the assumption of frame duration of 2.5 ms (for SCS = 60 kHz), the measurement rate of location relevant signal parameters will be 50 measurements in one second. The results are sent with this measurement rate to the location database within the RLC / PDCP protocols. The measured data arrive at the SDN FD as a PDCP packet, which are forwarded to the location database for processing.

The sequential measurement approach saves the number of parallel channels connecting RRLHC with RRLHs and eventually the number of mmWave modules. An alternative to selectively switch the 3.5 GHz IF successively to RRLH channel, which requires four 40 GHz IF to RF modules and a cheaper IF switch, as shown in Fig. 7a, is to selectively switch the 40 GHz RF successively to RRLH channel, which requires one 40 GHz IF to RF module, but more expensive RF switch, as shown in Fig. 7b. The option which will be realized depends on availability and the price of switches at 3.5 GHz and 40 GHz.

4.4 VLC UE position algorithms and integrated position protocol

In the case of VLC localisation, the RRLHC is a transmitter and the RSS of VLC signal is measured at UE side. The VLC location service is similar to the mmWave location service. According to the allocation of VLC positioning signal from Fig. 8, the last OFDM symbol of the first 4 sub-frames of 5G transport block is used to transmit an OFDM to only one of four RRLH VLC transmitters. Only one particular subcarrier frequency

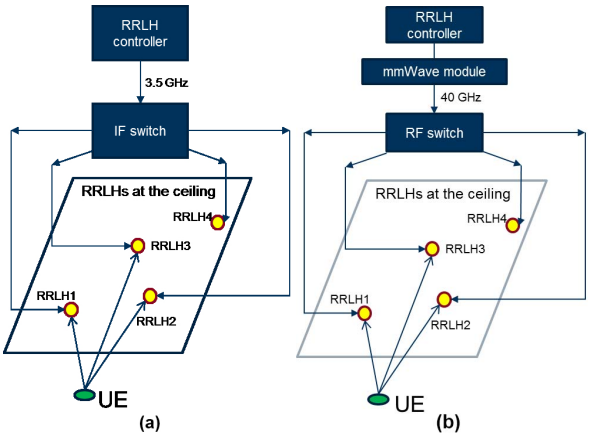

Fig. 7 Parameter estimation setup with IF switch (a) and RF switch (b).

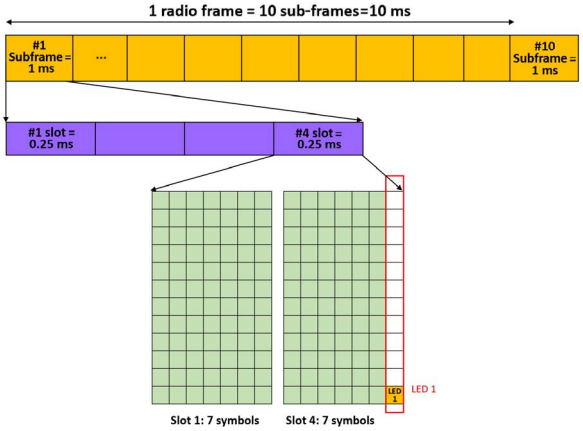

Fig. 8 Generation of VLC positioning signal in the generic 5G NR frame structure (SCS = 60 kHz) positioning procedure and location estimation.

is used to carry the reference positioning information of the corresponding LED lamp. This transmission is again preconfigured so that UE knows which RRLH is transmitting and uses the RSS information to estimate distance from it.

Since the IoRL project intends to use VLC LEDs of 10 MHz bandwidth and SCS of 60 kHz. This means that a measurement is obtained every 1 ms (1 slot duration)[15], which is sent at the VLC measurement result back to the location database every 8 ms using IP packets when averaged over 8 measurements.

The positioning procedure using the IPP protocol is described in Fig. 9. The central component is LD which contains three database tables. The first database table contains the measured location relevant signal parameter. The second one stores location coordinates of all connected UEs. The third database table contains location assistance data (LED and mmWave antenna coordinates). LD is accessed periodically by UE, RRLHC, and LS and on demand by LSC. This is indicated in Fig. 9 by periods T_{pos} and T_{estim} and aperiodic LSC readings of location estimates. T_{pos} represents the periodicity of RRLHC and UE access to LD. It is assumed that the period T_{pos} is long enough so that each RRLHC can perform sequential VLC measurements of all UEs connected to it. The period T_{estim} represents the periodicity of LS access to LD. Both T_{pos} and T_{estim} periods do not need to be equal. LS estimates location coordinates of all UEs connected to the IoRL system based on last parameter measurements saved in LDs.

The positioning procedure for both VLC and mmWave consists of the following parts:

(1) Measurement of location relevant parameters (runs continuously with the period T_{pos})

(a) RRLHC requests UE to start transmission of mmWave SRS and provides measurement assistance data (which SRSs and how many SRSs, etc.).

(b) UE synchronizes with one RRLH of the corresponding RRLHC. After UE and RRLHC lock their system clocks, respectively, UE starts transmission of SRS sequence (SRS1, SRS2, ..., SRSn). The sequences are sequentially received by the RRLHC switched mmWave architecture and used to estimate pToAs.

(c) UE requests RRLHC to start with the VLC RSS measurements.

(d) RRLHC sequentially transmits VLC sounding

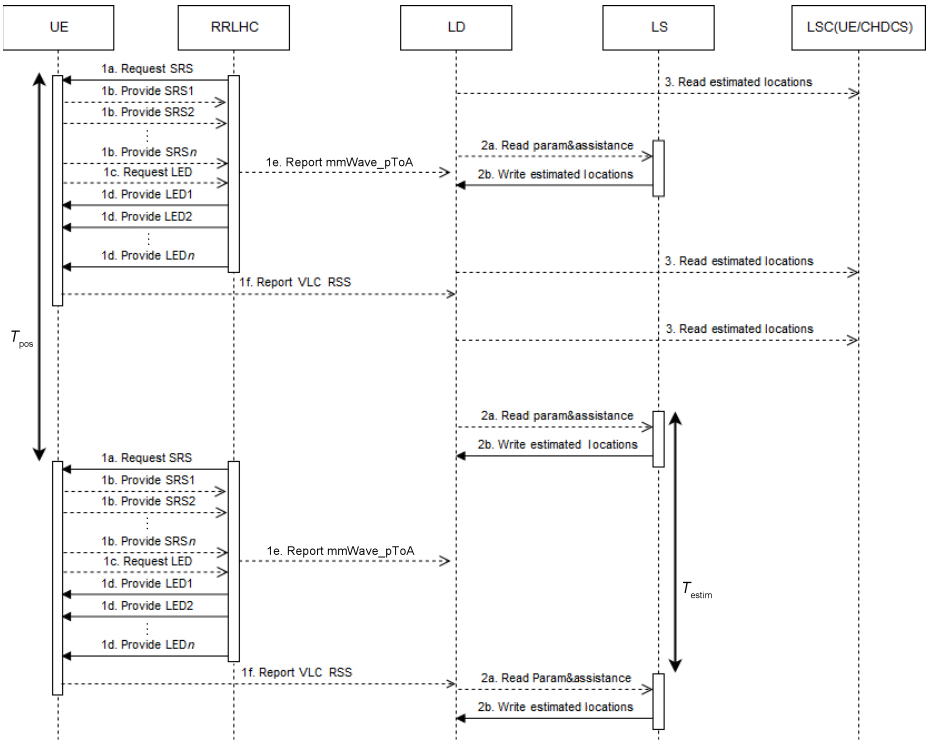

Fig. 9 Positioning procedure using IPP protocol.

signals using its LED1, LED2, . . ., LEDn.

(e) As far as RRLHC estimates pToA reports, it reports them to RRC which communicates the measurements to SDN by transferring mmWave pToAs to LD in the form of packets using PDCP protocol.

(f) UE estimates VLC RSS parameters related to each LED, UE's Android application SW transfers the VLC measurements to LD.

(2) Location estimation (runs continuously with the period T_{estim})

(a) LS reads location assistance data, VLC, and mmWave parameters from LD.

(b) LS writes results of the location estimation into LD.

(3) With the estimated locations, the LSC can read the location coordinates of all UE through the IoRL system on their own demands

In the case of IoRL demos, only preconfigured UEs and RRLHCs will be used. The IPP protocol will not be implemented, thus the positioning procedure is simplified to the one shown in Fig. 10. Compared with Fig. 9, there are only two differences in Fig. 10, i.e., (1) in Fig. 10, the RRLHC does not need to send request SRS message to obtain the Provide SRSn messages from UE; (2) in Fig. 10, the UE does not need to send request LED message to obtain the Provide LEDn messages from RRLHC. Otherwise, both procedures are very similar.

4.5 VLC-based location estimation algorithm

The RSS-based positioning algorithm is adopted to calculate the distance between RRLH lamps and UE by using the 3 highest strength of the Positioning Reference Signals (PRSs). A successful case has been presented in Ref. [16]. According to Lambertian radiation model, the VLC channel gain between the RRLH lamp and UE can be shown as

$$H(0) = \frac{(m+1)A\cos^m(\varphi)\cos(\theta)}{2d^2} \tag{1}$$

where φ is the radiation angle between the lamp and the UE, d is the distance between the lamp and the UE, A is the effective area of the receiver, and θ is the angle of light incident to the receiving surface of the detector. $\varphi_{1/2}$ is the half-power angle of lamp, and m is the order of Lambertian emission, which is relative to the semi-angle at half power of the lamp, i.e.,

$$m = \frac{-\ln 2}{\ln(\cos(\varphi_{1/2}))} \tag{2}$$

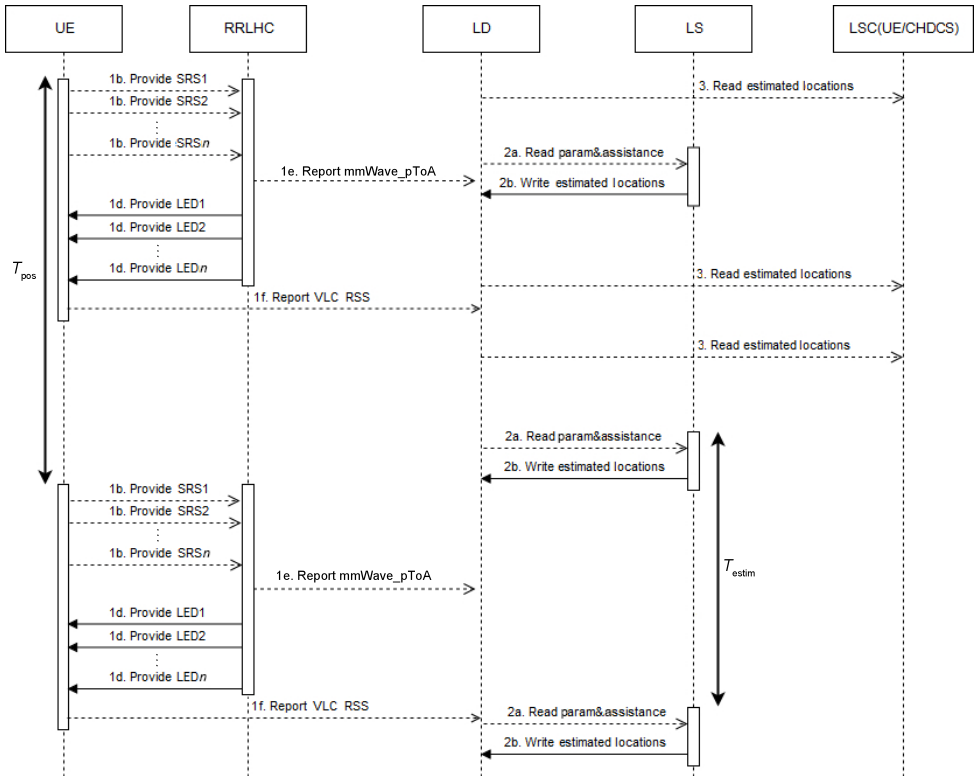

Fig. 10 Positioning procedure in the case of IoRL demos.

The received power P_{R} of the receiver can be shown as

$$P_{\mathrm{R}} = P_{\mathrm{T}} \frac{(m+1)A\cos^m(\varphi)\cos(\theta)}{2d^2} = P_{\mathrm{T}} \frac{(m+1)Ah^{m+1}}{2d^{(m+3)}} \tag{3}$$

where P_{T} is the transmitted light power of RRLH lamp and h is a known constant about the vertical distance between the UE and the LED lamp. The distance between the receiver and one lamp (ex. LED1) can be computed as

$$d_{\mathrm{LED1}\to R_x} = (m+3)\sqrt{\frac{(m+1)Ah^{(m+1)}}{2} \cdot \frac{P_{\mathrm{T}}}{P_{\mathrm{R}}}} \tag{4}$$

Similarly, the distance from the receiver to LED2 or LED3 can also be obtained. Based on this calculation, the projection distances r_1, r_2, and r_3 between RRLH lamps and receiver can be expressed as

$$r_1 = \sqrt{d_1^2 - h_1^2} \tag{5}$$

$$r_2 = \sqrt{d_2^2 - h_2^2} \tag{6}$$

$$r_3 = \sqrt{d_3^2 - h_3^2} \tag{7}$$

The estimated coordinates (x, y) thus can be calculated as follows:

$$\begin{cases} (x-x_1)^2 + (y-y_1)^2 = r_1^2, \\ (x-x_2)^2 + (y-y_2)^2 = r_2^2, \\ (x-x_3)^2 + (y-y_3)^2 = r_3^2 \end{cases} \tag{8}$$

where $(x_1, y_1), (x_2, y_2)$, and (x_3, y_3) are the coordinates of three RRLH lamps, respectively. Equation (8) can be formed in a matrix format as in Eq. (9), i.e.,

$$BX = C \tag{9}$$

where B, C, and X are defined as

$$B = \begin{bmatrix} x_2 - x_1 & y_2 - y_1 \\ x_3 - x_1 & y_3 - y_1 \end{bmatrix}, \quad X = \begin{bmatrix} x \\ y \end{bmatrix} \tag{10}$$

$$C = \begin{bmatrix} \dfrac{d_1^2 - d_2^2 + x_2^2 + y_2^2 - x_1^2 - y_1^2}{2} \\ \dfrac{d_1^2 - d_3^2 + x_3^2 + y_3^2 - x_1^2 - y_1^2}{2} \end{bmatrix} \tag{11}$$

The estimated receiver coordinates can be finally obtained by the linear least square as[17,18]

$$\hat{X} = (B^{\mathrm{T}}B)^{-1}B^{\mathrm{T}}C \tag{12}$$

4.6 mmWave-based location estimation algorithm

The mmWave positioning is based on TDOA estimates that are measured by RRLHs. Without loss of generality, let all the TDOA measurements $m_{i,1}$ be performed with respect to the first RRLH:

$$m_{i,1} = d_i - d_1 \tag{13}$$

where d_i $(i = 1, 2, \ldots, N)$ are unknown distances between the i-th RRLH and the UE. The UE coordinates can be computed by means of different approaches. Examples that are based on analytical, LS, Taylor series, approximate ML solution, or two-stage ML estimation are given in Refs. [19, 20]. The analytical and LS-based approaches are solving the following system of equations:

$$\begin{cases} (x-x_1)^2 + (y-y_1)^2 + (z-z_1)^2 = d_1^2, \\ (x-x_2)^2 + (y-y_2)^2 + (z-z_2)^2 = (d_1+m_{2,1})^2, \\ \quad \vdots \\ (x-x_N) + (y-y_N)^2 + (z-z_N)^2 = (d_1+m_{N,1})^2 \end{cases} \tag{14}$$

where the UE coordinate $[x, y, z]$ and d_1 are unknown variables that are to be estimated. In the case of only 4 RRLHs (the minimum constellation), an analytical solution is possible[19]. In the case of overdetermined system ($N > 4$), the LS solution leads to the UE position estimate[19]. The approach based on Taylor series linearizes a function which mathematically describes the TDOA range estimates:

$$f_i(x, y, z) = \sqrt{(x-x_i)^2 + (y-y_i)^2 + (z-z_i)^2} - \sqrt{(x-x_1)^2 + (y-y_1)^2 + (z-z_1)^2} \tag{15}$$

Expanding Eq. (13) into Taylor series by using an initial UE position estimate and keeping only the first two terms yield a system of linear equation that can be solved by LS method. The solution is used to iteratively refine the initial UE estimates as shown in Ref. [19]. Note that the performance of the location estimation depends on the constellation of received signal, the actual position of the UE, and the selected position estimation algorithm. In Ref. [19], it showed that there were significant differences in positioning error and availability of position estimates among various estimation algorithms.

5 Laboratory setup and configurations for transmission performance

5.1 5G NR frame structure design

To provide a comprehensive understanding of

the mmWave and VLC transmission performance measurement, a 5G radio frame design used for the mmWave and VLC transmission is described in detail in this section. Because the mmWave and VLC downlinks are the main research objects of this paper, only the downlink resource allocation is introduced. Meanwhile, to simplify the implementation, a fixed configuration is adopted in this system listed in Table 4.

An overview of a frame is introduced first. After that, the resource allocation of three channels: Physical Broadcast Channel (PBCH), PDCCH, and PDSCH, are discussed.

According to Table 4, the time domain allocation of one frame is shown in Fig. 11. As being seen in Fig. 11, one period of transmission takes 5 sub-frames. The first two sub-frames are used for Synchronization Signal (SS) and PBCH, and the following three sub-frames are for PDCCH and PDSCH. The second period starts at the 5th sub-frame and it takes another 5 sub-frames.

Figure 12 displays the resources allocation for two sets of SS/PBCH blocks in one slot and the allocation procedure follows the 5G specification[12].

Table 4 Fixed configuration of frame design.

Parameter	Value	Remark
Carrier frequency (GHz)	3.5	
Maximum bandwidth (MHz)	100	
Point *A* offset (kHz)	49 140	
Subcarrier space (kHz)	30	
Total number of resource blocks (RB)	273	
Cyclic prefix	Normal	
Number of sub-frames	10	Per frame
Number of slots	2	Per sub-frame
Number of symbols	14	Per slot
Time duration (ms)	0.5	Per slot

Note: Point *A* is the frequency point that indicates the distance from the centre frequency to the bottom boundary of 100 MHz bandwidth signal.

The Primary Synchronization Signal (PSS) and the Secondary Synchronization Signal (SSS) are used by UE to synchronize the system clock with the base station, identify the center frequency, and obtain the physical layer cell ID. The PDCCH and PDSCH are used for the control and data channel in the downlink separately. In time domain, the 0th symbol of each slot is allocated to PDCCH and the symbols from the first to 13th are reserved for PDSCH. In frequency domain of PDCCH, the resource blocks are assigned based on the parameters defined in Table 5. In IoRL system, the start point of the Control-Resource Set (CORESET) is set at the 48th RB and the size of CORESET is 24 RBs based on the Control Channel Elements (CCE) Aggregation Level (AL), which is 4 here, and the CCE size. The resource mapping of PDCCH Demodulation Reference Signal (DMRS) can be calculated based on the 5G specification[12]. Based on the configurations and calculation above, the PDCCH can be generated as shown in Fig. 13. For PDSCH, the configurations are defined in Table 6.

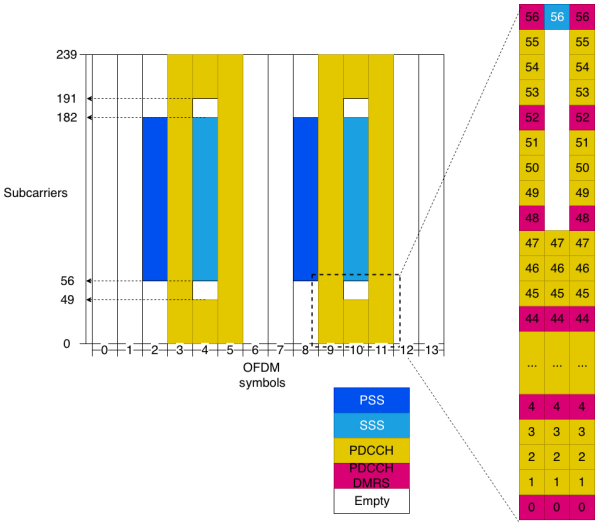

Fig. 12 Allocations of SS/PBCH in one slot.

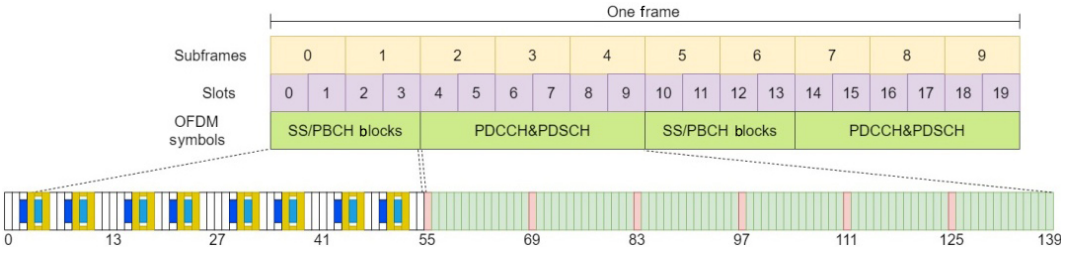

Fig. 11 Illustration of downlink frame structure.

Table 5 PDCCH configuration.

Parameter	Value	Remark
CORESET length	1 symbol	In time domain
CORESET mapping type	Non-interleave	
CCE size	6 RBs	In frequency domain
Number of PDCCH candidates	4	
CCE aggregation level	4	
Number of CCE	4	

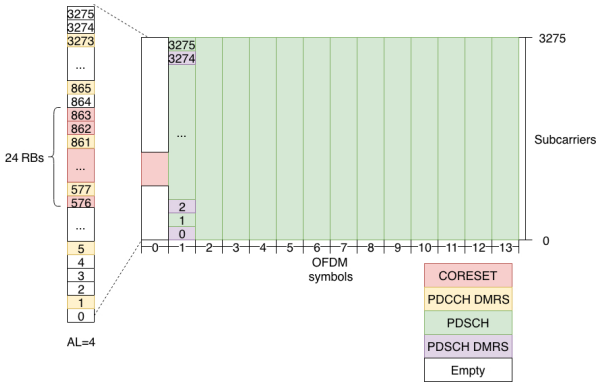

Fig. 13 Illustration of PDCCH and PDSCH.

Table 6 PDSCH configuration.

Parameter	Value	Remark
PDSCH RB size	273 RBs	In frequency domain
PDSCH start symbol	The first symbol	In time domain
PDSCH length	13 symbols	In time domain
PDSCH DMRS length	1 symbol	In time domain
PDSCH DMRS config type	Type 1	
PDSCH DMRS additional position	0	
PDSCH DMRS scramble ID	0	
Number of layers	3	

5.2 mmWave transmission testbed setup and configurations

The experiments are performed based on a commercial 5GNR testbed system running on the Ubuntu 14.04 server with a low-latency Linux kernel. The system communicates with Universal Software Radio Peripheral (USRP) through 10 Gigabit Ethernet cable. It is used to generate 3.5 GHz 5G radio signal for the mmWave TX. And it also delivers the received mmWave RX signal back to server. To make the TX and RX work with 60 GHz mmWave signal, a Local Oscillator (LO) generator is used to provide 14 GHz signal. A 10 MHz reference signal is supplied to both LO generator and the USRP. The system implementation and equipment are shown in Fig. 14. Because all experiments are performed in the indoor environment introduced above, an indoor channel model can be chosen to represent it. According to Refs. [21, 22], the key parameters that affect transmission performance in indoor environment are the path loss and multi-path propagation.

5.3 VLC transmission tested setup and configurations

The performance of VLC module is measured with lens and without lens as shown in Fig. 15. And the throughput of the VLC module is measured within the 5GNR UE Digital Signal Processor (DSP) with lens configured with different modulations. In this section, the test system setup and configuration are introduced firstly. The VLC transmission tested configurations are shown in Table 7. The experiments are performed based on the

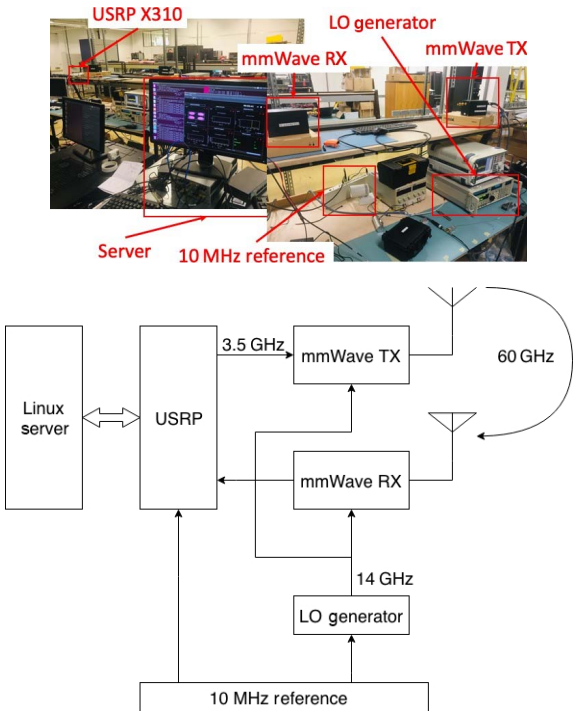

Fig. 14 mmWave transmission testbed setup.

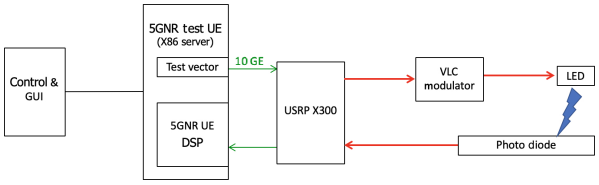

Fig. 15 VLC transmission testbed setup.

Table 7 VLC transmission testbed configurations.

Parameter	Value
TX/RX distance (m)	0.7
USRP gain (dBm)	0
Resource blocks	28 (about 10 MHz)
Number of time slots for PDSCH	15
Modulation Coding Scheme (MCS) table	2

Viavi 5GNR testbed system running on the Ubuntu 14.04 server with a low-latency Linux kernel. The Universal Software Radio Peripheral (USRP) is connected to the system with 10 Gigabit Ethernet cable for 5G VLC signal transmission. The signal will be sent through the VLC modulator and the LED light, and received by a photodiode.

6 Transmission performance measurement results

6.1 VLC transmission measurement

Because the VLC channel always suffers from fading and scattering problems in practice, we place a lens in front of the photodiode for gathering the LED light to improve the VLC performance. For this purpose, the Error Vector Magnitude (EVM) results with and without lens cases are compared and the screenshots of measurements are shown in Figs. 16 and 17, respectively. The EVM results of VLC with and without lens are 3.9% and 6.84%, respectively. According to these results, it is anticipated to decode the 256QAM signals successfully.

6.2 mmWave transmission measurement

(1) USRP transmit gain vs. EVM

The objective of this test is to measure the EVM with different USRP TX gains. Figure 18 shows the EVM of PDSCH and PBCH when the distance of USRP TX and RX is 7 m. And the minimum EVM requirements for Quadrature Phase Shift Keying (QPSK), 16QAM, 64QAM, and 256QAM are marked as dash lines in Fig. 18. The lowest EVM of PDSCH is 6.5% when USRP TX gain is 18 dBm. It can meet the EVM requirement of the 64QAM decoding. However, if we keep increasing USRP TX gain after that point, the higher USRP TX gain is, the worse the performance of PDSCH we get. The reason is that the excessive USRP TX gain makes the Peak to Average Power Ratio (PAPR) of OFDM system too high, causing the Power Amplifier (PA) nonlinear distortion which degrades the system's performance[12]. For PBCH, the lowest EVM is 3.3% with 22 dBm USRP TX gain. That is because the PBCH only occupies 239 subcarriers at most, which is not enough for the nonlinearity of PA.

Fig. 16 VLC EVM measurement with lens.

Fig. 17 VLC EVM measurement without lens.

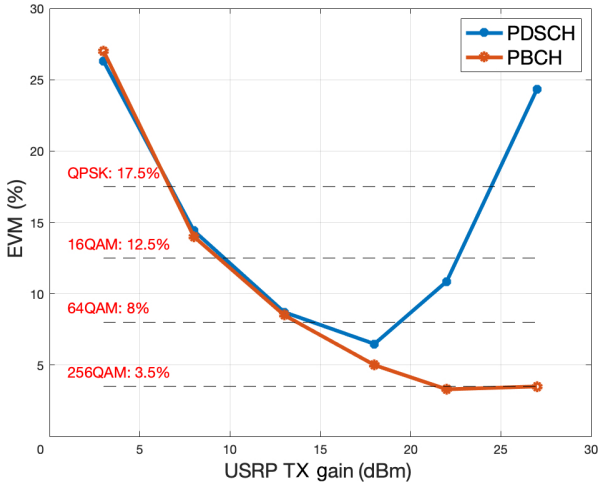

Fig. 18 EVM of PDSCH and PBCH with different USRP transmitting gains.

(2) Bandwidth vs. EVM

The EVM results of PDSCH and PBCH are measured with the bandwidths from 10 MHz to 100 MHz as shown

in Fig. 19. The EVM of PDSCH increases, while the mmWave is configured with higher bandwidth. The best EVM is 3.54% at 10 MHz bandwidth, which matches the 256QAM requirement. The worst is 6.03% at 100 MHz, which is still enough to decode 64QAM. The cause of the result is similar as mentioned in Section 6.2: The narrower bandwidth comes with less number of subcarriers, which make the PA work linearly.

For PBCH, the most of its EVM has a similar trend of the growth, but with much lower values, except with 10 MHz. At that point, the EVM is around 4.4%, which looks very unusual. It is probably because of the carrier leakage which causes a Direct Current (DC) offset or the I/Q imbalance problem[23] in the receiver. To find out the actual reason of it, more investigations and tests are needed in the future.

(3) USRP transmit gain vs. system throughput

To get the maximum transmission rate of mmWave, the throughput of system is measured with three types of modulation and coding schemes (see Fig. 20). From Fig. 20, the maximum throughput can reach 310 Mbit/s with 64QAM and code rate of 873/1024. The 256QAM case was also tested, but the signal cannot be decoded because the EVM did not meet the requirement.

(4) Distances

To find out the impact of distance between TX and RX, three distances are tested with three USRP TX gains (see Fig. 21). From Fig. 21, for 7 m, according to Section 6.2, the best USRP TX gain is 18 dBm and its EVM is around

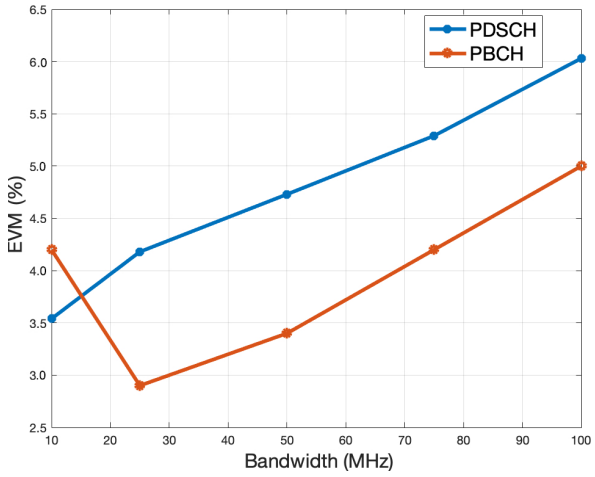

Fig. 19 EVM of PDSCH and PBCH with different bandwidths.

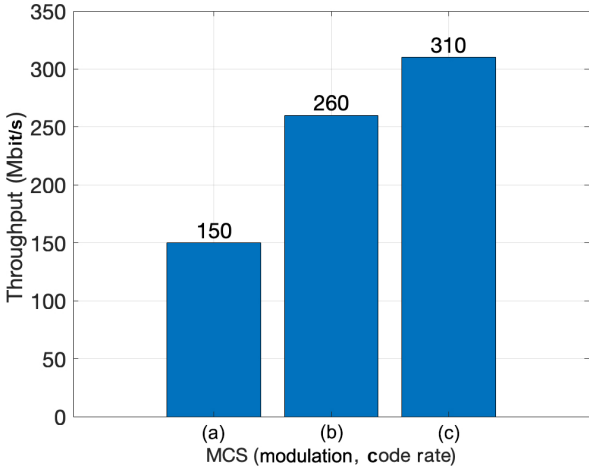

Fig. 20 System throughput of PDSCH with different modulation coding schemes: (a) 16QAM, code rate of 616/1024; (b) 64QAM, code rate of 719/1024; and (c) 64QAM, code rate of 873/1024.

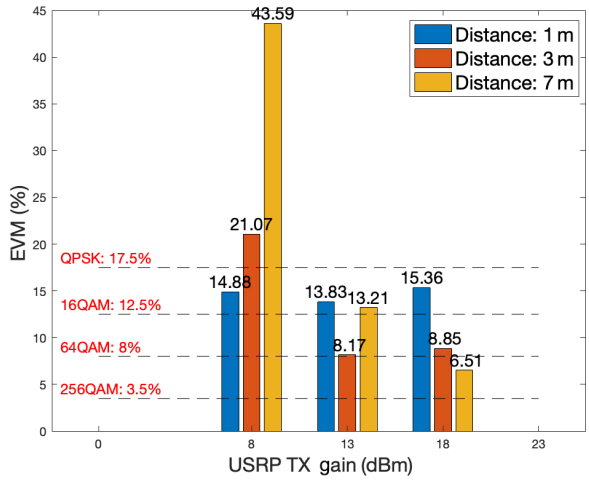

Fig. 21 EVM of PDSCH with different TX/RX distances.

6.5%. The EVM increases with short distances, because the signal power is too high. The best USRP TX gain for both 3 m and 1 m scenarios is 13 dBm. For 1 m scenario, the EVM is barely affected by distances and the results of three different USRP TX gains are quite close. This scenario needs more tests with different USRP TX gains in the future.

7 Positioning sensing simulation

7.1 mmWave positioning sensing simulation

The simulation scenario is shown in Fig. 22. Eight RRLHs were aligned in two rows in a rectangular room.

Geometric Dilution Of Precision (GDOP) is a term mainly used in satellite navigation to specify how

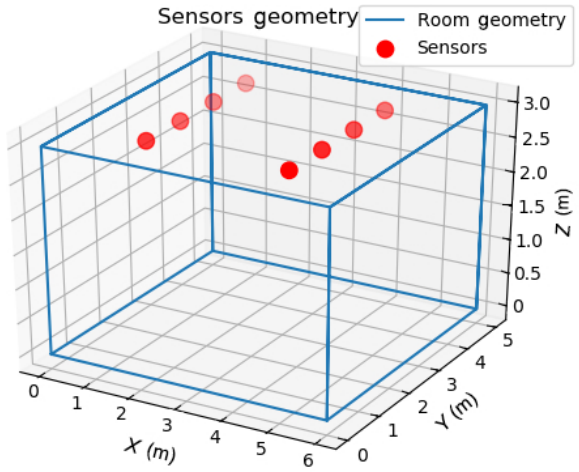

Fig. 22 mmWave positioning simulation scenario with 8 RRLHs aligned in two rows.

errors in the measurement will affect the final location estimation. The output of the GDOP analysis is usually a heat map which indicates the positioning precision at a specific location of a target by using a specific sensor topology.

A simulation result of a two-dimensional heat map that is based on the GDOP computation by means of the Taylor series is illustrated in Fig. 23.

According to the RRLH constellation, the UE had a fixed height of 1 m and the Standard Deviation (STD) of the noise that corrupted the ideal TDOAs was only 10 cm. Despite these, this TDOA error is propagated up to almost 2 m positioning error.

A more detailed description in the decomposed GDOP (see Fig. 24) suggests the reason of this poor positioning precision. The main axis of the ellipsoid reaches value

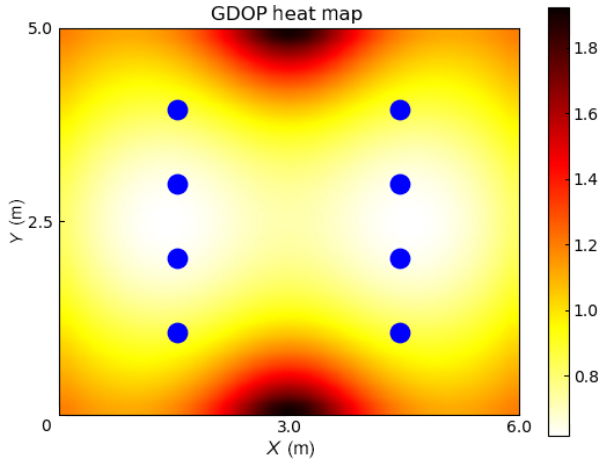

Fig. 23 mmWave positioning simulation result of GDOP for an RRLH constellation with 8 RRLHs.

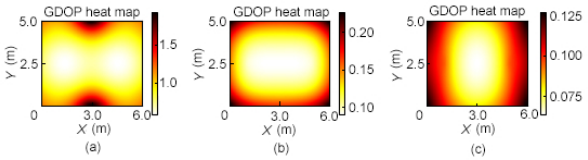

Fig. 24 Decomposed GDOP of 8 RRLHs into the main axes of the ellipsoid.

up to almost 2 m, while the remaining two axes reach only small values that are less than 20 cm, which are in line with the TDOA STD of 10 cm. The reason for that is the symmetric RRLH distribution with RRLHs situated in one plane. This affects mainly the resolution in the Z-coordinate of the UE. Increasing the number of RRLHs will not help to improve the localization precision. A possible way to improve the localization precision is to optimize the RRLH distribution.

7.2 VLC positioning sensing simulation

A Python-based VLC position sensing simulator Graphical User Interface (GUI) is developed in location server. This GUI features a user-friendly graphical interface including options for setting up irregularly shaped indoor scenarios, e.g., oval offices and triangle rooms, as shown in Fig. 25.

It is designed to perform the positioning algorithm, set up the location assistance data, and display the measurement parameter and location estimation result. Thanks to this application, the location assistance data, such as Lambertian factor, transmitted power, and receiving area of photodiode, could be easily configured according to the different practical experimental conditions, such as the coordinates of RRLH lamps, the characteristic of RRLH lamps or the dimension of room.

The lab simulation is performed to test our positioning system. It simulates indoor optical multipath channels with 4 transmitters and 1 receiver, and the simulation settings are summarized in Table 8.

The VLC power received by the UE device can obtain an estimated distance between the UE and the LED. With the location of the LED, the estimated location of the UE can be calculated by measuring the RSS at each available UE. The test subject moved in curve on the ground, as can be seen in Fig. 26 at different position points. 95% of the performed simulation tests showed position error within 10 cm. A further optimization could be provided

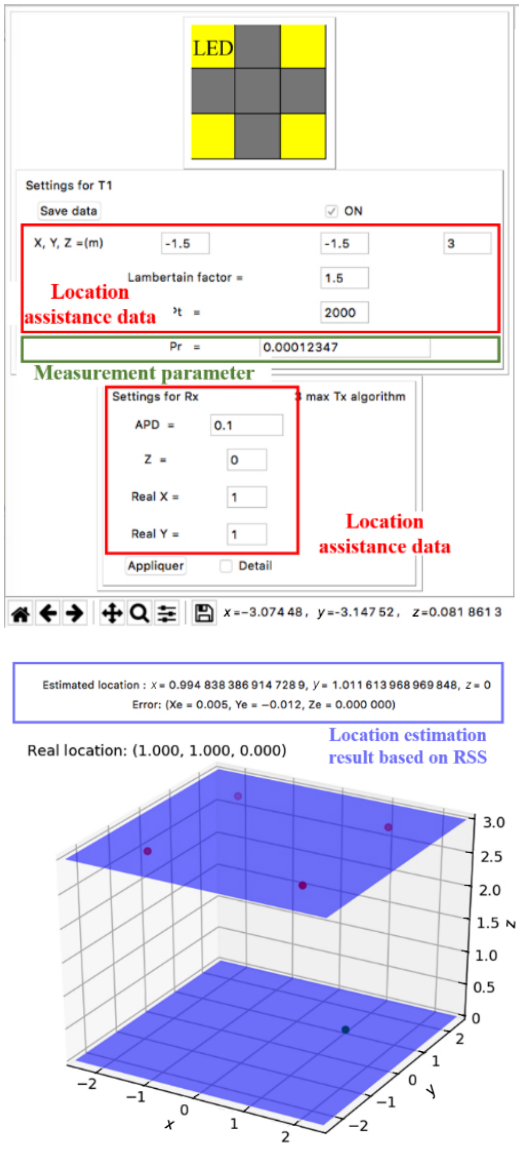

Fig. 25 GUI of VLC-based positioning for indoor environment configuration (top) and position simulation result (bottom).

by combining with the mmWave positioning sensing method to achieve a higher positioning accuracy less than 10 cm.

8 Conclusion

This paper presents a new 5G radio and edge architecture for indoor environments based on the IoRL system architecture. We show how the system can utilise reconfigurable RAN setting, SDN concepts of configurable traffic routing reactively, and NFV technology for enabling flexible service deployment and

Table 8 Laboratory environment setting and parameters.

Parameter	Value
Lab dimension (m)	5 (W) × 5 (L) × 3 (H)
Reflection coefficient of wall ρ_{wall}	0.66
Reflection coefficient of ceilling ρ_{ceilling}	0.35
Reflection coefficient of floor ρ_{floor}	0.6
Lambertian mode of transmitter (m)	1
Elevation of transmitter (°)	−90
Azimuth of transmitter (°)	0
Effective area of receiver ∅ (mm)	7.00
Height of receiver (cm)	17.50
Elevation of receiver (°)	+90
Azimuth of receiver (°)	0
FOV of receiver (°)	60
Photosensitivity of receiver (A/W)	0.42

exploiting the huge bandwidth and location estimation accuracy offered by the IoRL system. For instance, we explain that IoRL devises a layered architecture consisting of three layers, i.e., service, NFV/SDN, and access layer, and the architecture can well align to the overall 5G architecture. We also discuss the improvements to the 5G remote radio head architecture made by including VLC, mmWave module, and RRLH. The multi-component carrier feature of 5G architecture is used to transmit at these two different parts of the EM spectrum. The impact of this is that the total throughput to a building can potentially be dramatically increased. And an RAN architecture is developed that processes the 5G lower Layer 1, upper Layer 1, and Layers 2 and 3 protocol stack in a parallel pipeline interconnected by a 10 Gbit/s Ethernet ring. The paper delivers the IoRL position service architecture for VLC and mmWave as well the algorithms estimating the location of UE which are developed using a combination of the RSS of VLC OFDM reference symbols and round trip times of mmWave OFDM reference symbols. White LED lamps and commercial Avalanche Photodiode (APD) show that the system has a high data rate of around 45.25 Mbit/s in the laboratory environment and a mean PE of 0.18 m. With mmWave, the performance improvement in the case of the worst UE places in the room is about 30% (47 cm vs. 33 cm). The best achieved localization performance also improves from about 24 cm to about 17 cm. Such positioning accuracy meets

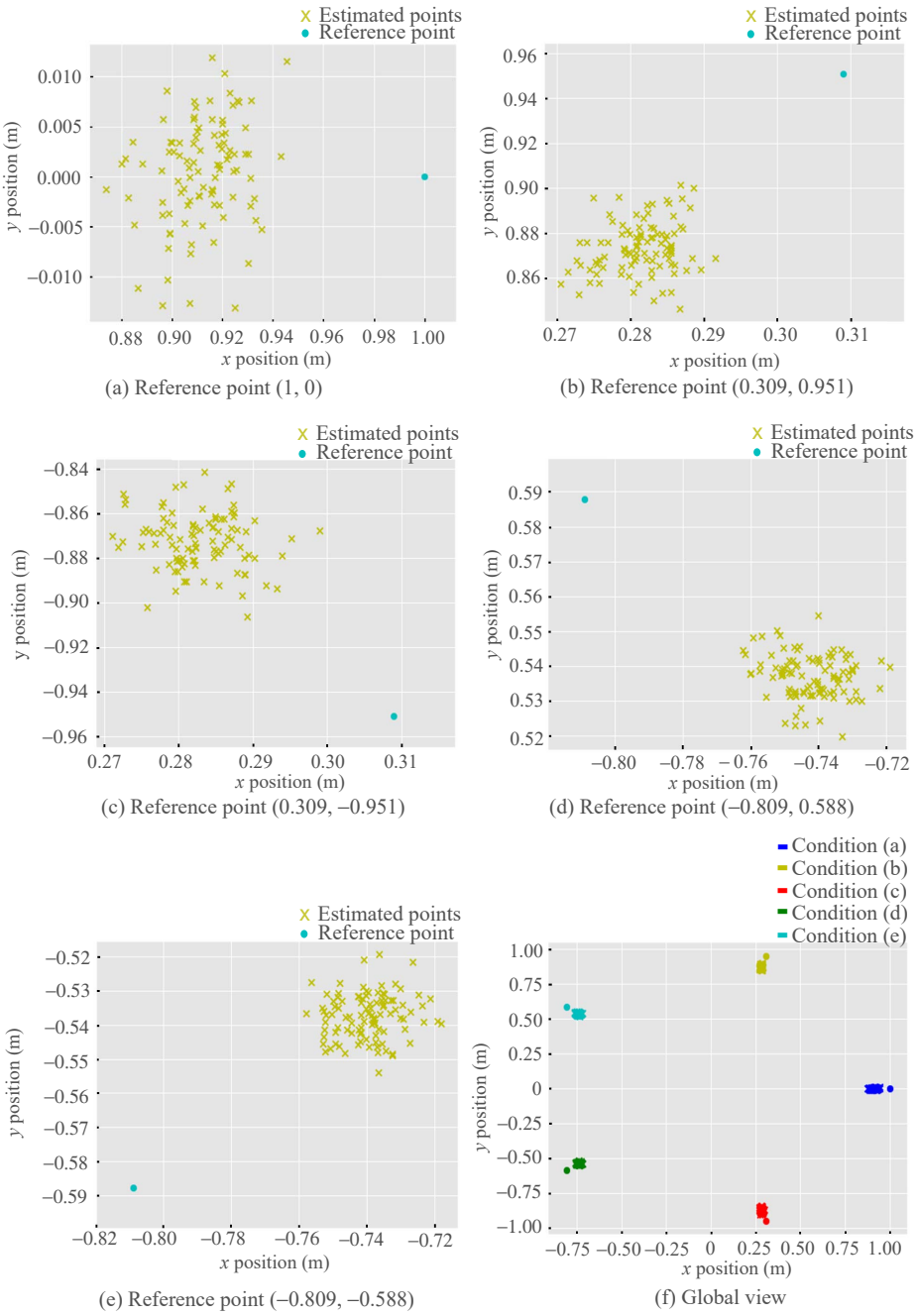

Fig. 26 VLC location estimation on different positions.

the 5G indoor positioning requirement well. Besides that, the system has many other excellent features, such as high communication bandwidth, high-capacity, and radiation-free.

The EVM performance and the system throughput of the mmWave and VLC for IoRL RAN and edge architecture are measured in different configurations and scenarios. According to the results discussed in the previous section, the maximum throughput of the current system is 310 Mbit/s with 64QAM and 873/1024 code rate. And based on the results, the EVM performance can be effected by the TX gain, the maximum bandwidth as well as the distance and the angles between TX and RX antennas. The best USRP TX gains for 7, 3, and 1 m scenarios are 18, 13, and 13 dBm, respectively. With those TX gains, the mmWave system can decode 64QAM at 7 m and 3 m scenarios, and decode QPSK at 1 m scenario. Different bandwidth settings can also affect

the EVM. So, it is possible to reduce the bandwidth to obtain a better EVM performance in some cases. Based on the EVM results of TX/RX angles, the mmWave only has 30° available transmission range. The radiation pattern of an mmWave transmitter with a horn antenna is directional. However, the objective of the IoRL project is to equally illuminate a room with a radiation pattern since UEs can be located anywhere within a room. Therefore, experiments will be repeated without the horn antenna that more equally illuminate the room with the patch antenna radiation pattern.

Acknowledgment

This work was supported by the National Key R&D Program of China (No. 2017YFE011230) and the EU Horizon 2020 Project (No. 761992).

References

[1] L. Ge, G. J. Chen, Y. Zhang, J. Tang, J. T. Wang, and J. A. Chambers, Performance analysis for multihop cognitive radio networks with energy harvesting by using stochastic geometry, *IEEE Internet of Things Journal*, vol. 7, no. 2, pp. 1154–1163, 2020.

[2] L. J. Ge, Y. Zhang, G. J. Chen, and J. Tong, Compression-based LMMSE channel estimation with adaptive sparsity for massive MIMO in 5G systems, *IEEE Systems Journal*, vol. 13, no. 4, pp. 3847–3857, 2019.

[3] H. Luo, Y. Zhang, L. K. Huang, J. Cosmas, and A. Aggoun, A closed-loop reciprocity calibration method for massive MIMO in terrestrial broadcasting systems, *IEEE Transactions on Broadcasting*, vol. 63, no. 1, pp. 11–19, 2017.

[4] N. Jawad, M. Salih, K. Ali, B. Meunier, Y. Zhang, X. Zhang, R. Zetik, C. Zarakovitis, H. Koumaras, M. A. Kourtis, et al., Smart television services using NFV/SDN network management, *IEEE Transactions on Broadcasting*, vol. 65, no. 2, pp. 404–413, 2019.

[5] J. Cosmas, Y. Zhang, and X. Zhang, Internet of radio-light: 5G broadband in buildings, presented at European Wireless 2017-23rd European Wireless Conf., Dresden, Germany, 2017.

[6] J. Cosmas, B. Meunier, K. Ali, N. Jawad, M. Salih, H. Y. Meng, J. Song, J. T. Wang, M. Tong, X. H. Cao, et al., 5G internet of radio light services for supermarkets, presented at 2017 14th China International Forum on Solid State Lighting: International Forum on Wide Bandgap Semiconductors China (SSLChina: IFWS), Beijing, China, 2017, pp. 69–73.

[7] J. Cosmas, B. Meunier, K. Ali, N. Jawad, M. Salih, and H. Y. Meng, A scaleable and license free 5G Internet of radio light architecture for services in train stations, presented at European Wireless 2018-24th European Wireless Conf., Catania, Italy, 2018.

[8] Q. B. Bai, J. T. Wang, Y. Zhang, and J. Song, Deep learning-based channel estimation algorithm over time selective fading channels, *IEEE Transactions on Cognitive Communications and Networking*, vol. 6, no. 1, pp. 125–134, 2020.

[9] 3GPP, NR; User Equipment (UE) radio transmission and reception; Part 1: Range 1 Standalone, http://www.3gpp.org/DynaReport/38101-1.htm, 2019.

[10] S. Perrin, Evolving to an open C-RAN architecture for 5G, https://www.fujitsu.com/us/Images/FNC-Fujitsu-Evolving-to-an-Open-C-RAN-Architecture-for-5G-White-Paper.pdf, 2017.

[11] L. Shi, W. Li, X. Zhang, Y. Zhang, G. J. Chen, and A. Vladimirescu, Experimental 5G new radio integration with VLC, presented at 2018 25th IEEE Int. Conf. Electronics, Circuits and Systems (ICECS), Bordeaux, France, 2018, pp. 61–64.

[12] 3GPP TS 38.211 V1.0.0, Physical channels and modulation, http: //www.3gpp.org/ftp//Specs/archive/38_series/38.211/38211-100.zip, 2017.

[13] 3GPP TS 38.104 V1.0.0, Base Station (BS) radio transmission and reception, http://ftp.3gpp.org//Specs/archive/38_series/38.104/38104-100.zip, 2017.

[14] 3GPP TS 38.211 V15.4.0, Physical channels and modulation, http://www.3gpp.org/ftp//Specs/archive/38_series/38.211/38211-f40.zip, 2018.

[15] R. Abbas, K. Michael, and M. G. Michael, Location-based privacy, protection, safety, and security, in *Privacy in a Digital, Networked World*, S. Zeadally and M. Badra, eds. Springer International Publishing, 2015, pp. 391–414.

[16] H. S. Mousavi, V. Monga, and T. D. Tran, Iterative convex refinement for sparse recovery, *IEEE Signal Processing Letters*, vol. 22, no. 11, pp. 1903–1907, 2015.

[17] H. S. Mousavi, U. Srinivas, V. Monga, Y. M. Suo, M. Dao, and T. D. Tran, Multi-task image classification via collaborative, hierarchical spike-and-slab priors, in *2014 IEEE Int. Conf. Image Processing (ICIP)*, Paris, France, 2014, pp. 4236–4240.

[18] J. Bruneau-Queyreix, M. Lacaud, D. Negru, J. M. Batalla, and E. Borcoci, MS-Stream: A multiple-source adaptive streaming solution enhancing consumer's perceived quality, presented at 2017 14th IEEE Annu. Consumer Communications & Networking Conf. (CCNC), Las Vegas, NV, USA, 2017, pp. 427–434.

[19] G. W. Shen, R. Zetik, and R. S. Thoma, Performance comparison of TOA and TDOA based location estimation algorithms in LOS environment, presented at 2008 5th Workshop on Positioning, Navigation and Communication, Hannover, Germany, 2008, pp. 71–78.

[20] R. M. Buehrer, H. Wymeersch, and R. M. Vaghefi, Collaborative sensor network localization: Algorithms and

practical issues, *Proceedings of the IEEE*, vol. 106, no. 6, pp. 1089–1114, 2018.

[21] L. F. Feng, H. B. Yang, R. Q. Hu, and J. P. Wang, mmWave and VLC-based indoor channel models in 5G wireless networks, *IEEE Wireless Communications*, vol. 25, no. 5, pp. 70–77, 2018.

[22] K. Haneda, J. Järveläinen, A. Karttunen, M. Kyrö, and J. Putkonen, A statistical spatio-temporal radio channel model for large indoor environments at 60 and 70 GHz, *IEEE Transactions on Antennas and Propagation*, vol. 63, no. 6, pp. 2694–2704, 2015.

[23] W. Li, Y. Zhang, L. K. Huang, J. Cosmas, C. Maple, and J. Xiong, Self-IQ-demodulation based compensation scheme of frequency-dependent IQ imbalance for wideband direct-conversion transmitters, *IEEE Transactions on Broadcasting*, vol. 61, no. 4, pp. 666–673, 2015.

Yue Zhang is an associate professor at Department of Engineering, University of Leicester. He received the BE and ME degrees from Beijing University of Post and Telecommunications in 2001 and 2004, respectively. In 2008, he received the PhD degree from Brunel University, UK where he also worked as a research engineer for the EU FP6 project—PLUTO. From 2008, he was a signal processing design engineer at Microwave Measurement Division-Europe, Anritsu Corp. He was responsible for the RF/IF and digital and DSP design for the measurement instruments for various wireless and broadcasting systems. From 2010, he joined Department of Computer Science and Technology, University of Bedfordshire, Luton, UK as the reader in signal processing. He also worked at Royal Academy of Engineering, UK and Industrial Fellowship with Aeroflex Ltd. He currently leads EU Horizon 2020 5GPPP project IoRL as the innovator and the most important workpackage leader. He is also one of the commitee members of 5G PPP pre-standardization and 5G Architecture WG. His research interests are signal processing for 5G wireless and mobile systems, radio propagation model and multimedia, and wireless networks. He currently serves as the associate editor for *IEEE Transactions on Broadcasting* and *IEEE Access*.

John Cosmas received the BEng degree in electronic engineering from Liverpool University in 1978 and the PhD degree from University of London in 1986. He is currently a professor of multimedia systems at the College of Engineering, Design and Physical Sciences, Brunel University London. He leads the 5G and Beyond Research Centre and is an associate editor of *IEEE Transactions on Broadcasting*. His research interests are concerned with the development of multimedia networked systems applied to future of broadcasting, cellular communications, 2D/3D digital video/graphics media and the synergies between these technologies towards their application towards the benefit of the smart homes, cities environment, health, and societies. He has participated in twelve EU (Horizon 2020, IST, RACE, and ACTS) research projects and two EPSRC funded research projects since 1986, and led three of these (CISMUNDUS, PLUTO, and 3D MURALE). He has graduated 35 PhD and 4 MPhil students and published over 89 research journal papers and 198 conference papers. He leads a research team of 5 PhD students, whose research is concerned with management of heterogeneous visible light communications and millimetre wave networks for low latency broadband in buildings, internet of things for health and safety systems in hospitals 3D MIMO, and efficient software defined networks architectures.

Hequn Zhang received the master's degree in computer science and engineering from Halmstad University, Sweden in 2014. He is now a PhD student in wireless communication at University of Leicester, UK. His main research area involves channel measurement and modelling, NOMA/LDM, and index modulation technologies for 5G wireless network. Since 2018, he has been working on the mmWave/VLC channel measurement and implementation of 5G Layer 2 protocols in the IoRL project which is supported by European Commission Horizon 2020 Programme.

Nawar Jawad received the master's degree in wireless communication systems from Brunel University London, UK in 2009. He is now a PhD student in wireless communication systems at Brunel University London, UK. His main research area involves cloud computing and designing intelligent services for the end users. Since 2017, he has been working on designing an Intelligent Home IP Gateway (IHIPGW) for 5G indoor coverage network utilizing OpenStack virtual infrastructure manager and integrating the services in the form of VNFs, along with essential services to route the traffic efficiently amongst the available links.

Jintao Wang received the BEng and PhD degrees in electrical engineering from Tsinghua University in 2001 and 2006, respectively. From 2009 to 2019, he was an associate professor at Department of Electronic Engineering, Tsinghua University, where he has been a professor and a PhD supervisor since 2019. He has published more than 160

journal and conference papers and holds more than 50 national invention patents. His current research interests include MIMO, OFDM, and channel estimation and equalization techniques. He was the TPC co-chair of the *IEEE International Symposium on Broadband Multimedia Systems and Broadcasting* from 2013 to 2020.

Kareem Ali received the bachelor's degree in computer systems engineering from Brunel University London, UK in 2017. Now he is a doctoral researcher, where his main area of research involves the development of 5G applications. Since 2017, he has been working on development of 5G indoor location data access and indoor monitoring and guiding.

Ben Meunier received the bachelor's degree in electronic and electrical engineering from Brunel University London, UK in 2017. He is currently working as a doctoral researcher within the Horizon 2020 Internet of Radio Light (IoRL) project, focusing on the enhancement of Virtual Reality (VR) systems through 5G networks. His work includes the proposal and analysis of hybrid localization techniques for VR tracking as well as development of the IoRL location server.

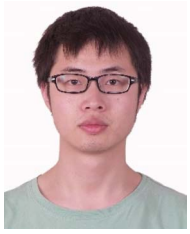

Wei Li is the algorithm engineer at Viavi Solutions. He specializes in physical layer design/implementation for 5G wireless system. He is responsible for physical/MAC layer design and integration of new products at Viavi. He is also responsible for technique development and research in H2020 project Internet of Radio Light (IoRL).

Lina Shi received the master's degree in computer science and electronics for embedded systems from Université Grenoble Alpes, France in 2017. She is now a PhD student in visible light communication at Institut Supérieur D'électronique De Paris, France. Her main research area involves implementation and optimization of visible light communication system convergence in 5G network. Since 2018, she has been working on the VLC measurement and implementation in the EU Horizon 2020 5G IoRL project.

Xun Zhang received the PhD degree in electrical engineering from Nancy University, France in 2009. From 2011 to 2020, he was an associate professor and PhD supervisor at the Department of Electronic Engineering, Institute Suprieur dlectronique Paris (ISEP). He has published more than 100 journal and conference papers and book chapters. His current research interests include OWC, VLP, OFDM, and physical layer power efficient design in wireless commutation system.

Israel Koffman received the MSc degree in electrical engineering from Drexel University and the BSc degree in electrical engineering from Technion, Haifa, Israel. He is an expert in cellular networks (5G/4G), PHY/MAC, satellite communication, fixed wireless communications, interactive TV, broadcasting, tracking and telemetry, RF systems and antennas as well as strategic marketing plans, Marcom, marketing documentation, marketing research, representation and distribution agreements, VAR agreements, OEM agreements, and more. Prior to joining RunEL, he served as CEO and marketing and sales manager in Runcom as well as CTO at Gilat Satellite Networks and CEO at Orbit Communications. As the marketing and sales manager in Runcom, he led a cumulative amount of 80 million Euros sales to global Tier-1 cellular companies, such as Samsung (Korea), Motorola (USA), Nortel (Canada), Alcatel (France), Huawei (China), SK Telesys (Korea), Ultra (Canada), and more.

Charilaos C. Zarakovitis received the BSc, two MScs, an MPhil, and PhD degrees in electronic engineering. He has academic experience gained at NCSRD GR, TEI Piraeus GR, ULancaster UK, USurrey UK, UBrunel UK, and DIT IE as well as industrial experience gained at Motorola UK and Intracom GR, where he offered services in scientific research and development. His research interests include the design and decision-making in green communications systems, cyber physical systems, cognitive radios, visible light communications systems, vehicular networks, neural networks, in the sense of developing novel and optimised solutions based on distributed computing, machine learning, evolutionary bio-inspired computation, network virtualisation, system and control theory, game theory, probability theory, and quantum theory and convex analysis. His publications in these fields have attracted 500+ citations, with the H-index of 8.